Supplementary Material: Modelling glacier mass balance and runoff in the Kaskawulsh River headwaters of southwest Yukon, Canada, 1980–2022

Katherine M. Robinson[1], Gwenn E. Flowers[1], Michel Baraër[2], David R. Rounce[3]

[1]*Department of Earth Sciences, Simon Fraser University, Burnaby, BC, Canada*

[2]*Département de génie de la construction, École de Technologie Supérieure, Montréal, QC, Canada*

[3]*Civil and Environmental Engineering Department, Carnegie Mellon University, Pittsburgh, PA, USA*

Correspondence: Katherine Robinson <kmr18@sfu.ca>

CONTENTS

1 MASS-BALANCE MODEL DESCRIPTION

The climatic mass balance $\dot{b}_{\mathrm{sfc}}(x, y)$ is calculated as the difference between surface accumulation and surface ablation $\dot{a}_{\mathrm{sfc}}(x, y)$. Ablation is approximated as surface melt (M; m w.e.) minus meltwater that is refrozen (R; m w.e.). Melt is calculated using the enhanced temperature-index model of Hock (1999),

$$M = \begin{cases} (MF + a_{\mathrm{snow/ice}} I)T & \text{if } T > 0\,^{\circ}C \\ 0 & \text{if } T \leqslant 0\,^{\circ}C, \end{cases} \tag{1}$$

where T (°C) is air temperature and I is the potential direct clear-sky solar radiation (W m^{-2}), calculated using the Hock (1999) shading module, which accounts for the effects of topographic shading, slope, and aspect. MF (m w.e. 3hr^{-1} °C^{-1}), a_{snow} and a_{ice} (m w.e. 3hr^{-1} °C^{-1} m^2 W^{-1}) are, respectively, the melt factor and radiation factors for snow and ice that are empirically determined during the tuning process.

The retention of meltwater via percolation and refreezing in the snowpack is accounted for using a thermodynamic parameterization to estimate the maximum amount of liquid water that can be retained, referred to as the total potential retention mass P_τ (m w.e.) (Janssens and Huybrechts, 2000). P_τ is approximated as a proportion (P_{r}) of the total annual precipitation in a given hydrological year (P_{annual}; m w.e.):

$$P_{\mathrm{r}} = \frac{c}{L} |\min(T_{\mathrm{mean}}, 0)| \frac{d}{P_{\mathrm{mean}}}, \tag{2}$$

where c (2097 J kg^{-1} K^{-1}) is the specific heat capacity of ice, L (333.5 kJ kg^{-1}) is the latent heat of fusion Cuffey and Paterson (2010), T_{mean} is the local mean annual air temperature for a given hydrological year, P_{mean} (m w.e.) is the mean annual precipitation over the whole study period (1980–2022), and d is a prescribed thickness of the thermal active layer, set to 2 m (Janssens and Huybrechts, 2000; Young and others, 2021). The retention fraction P_r can have a maximum value of 1, such that the maximum possible potential retention mass P_τ is equal to the annual precipitation (P_{annual}), since

$$P_\tau = P_r \, P_{\mathrm{annual}}. \tag{3}$$

While $\mathrm{P}_\tau > 0$, any melt that occurs is assumed to refreeze, therefore the maximum amount of refreezing that can occur is capped at P_τ. Once the upper limit of P_τ has been reached, any additional snowmelt or rainfall is assumed to run off (Huybrechts and De Wolde, 1999; Janssens and Huybrechts, 2000).

2 CATCHMENT HYPSOMETRY

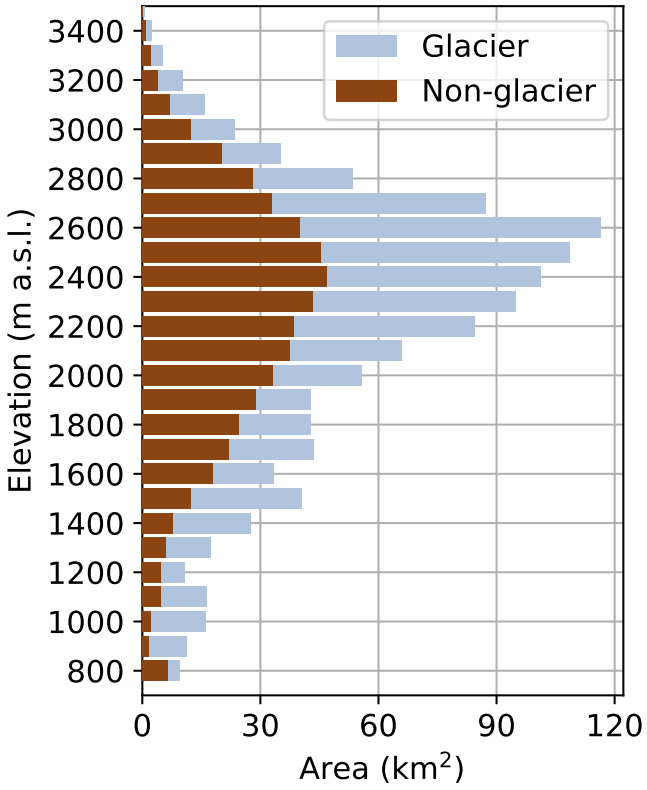

Fig. S1. Hypsometry of the Kaskawulsh River headwaters. Glacierized areas (light blue bars) account for 69% (1173 km^2) of the catchment area, while the other 31% (531 km^2) of the catchment is non-glacierized (brown bars).

3 AVERAGE CUMULATIVE MASS BALANCE CURVE AND ONSET OF NET ABLATION

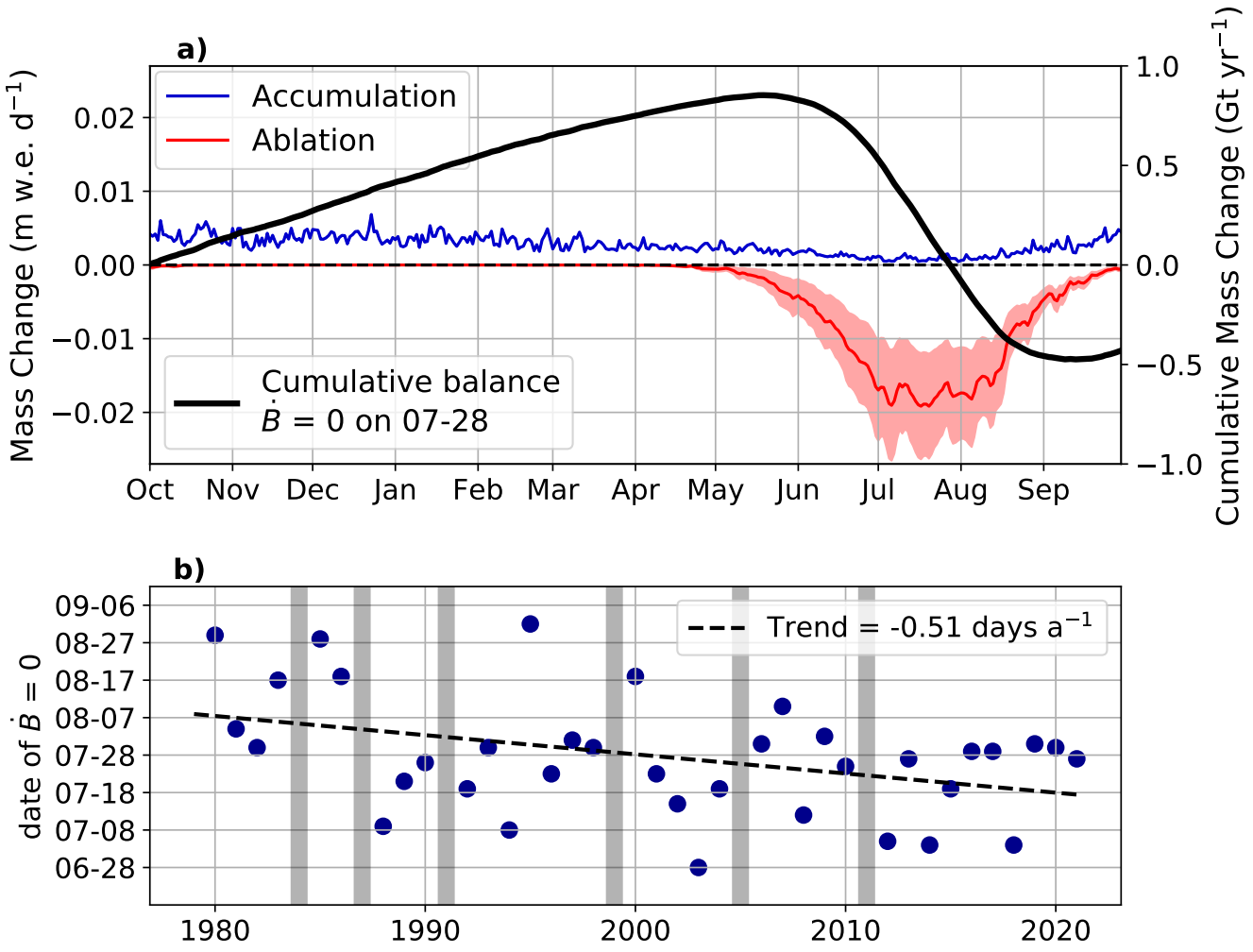

Fig. S2. a) Average accumulation (blue), ablation (red), and cumulative mass balance (black) from 1980–2022 for the glacierized area of the Kaskawulsh River Headwaters catchment. Red shading on the ablation timeseries shows $\pm 1\,\sigma$ of variability in the 100 simulations that comprise the model. The average onset of net ablation (where $\dot{B} = 0$) is July 28. b) The date when $\dot{B} = 0$ during each mass balance year. The onset of net ablation is occurring earlier in the melt season by approximately five days per decade. Grey bars represent years where the cumulative balance remains positive for the entire year.

4 OBSERVED DISCHARGE ON THE ALSEK RIVER (1979–2019)

4.1 Annual discharge on the Alsek River above Bates River

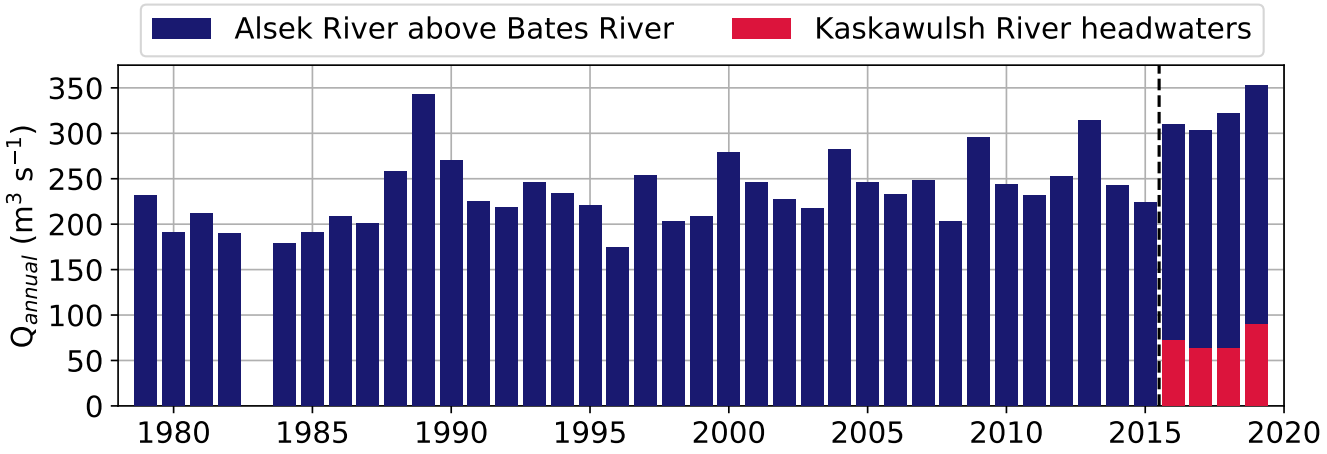

Fig. S3. Annual discharge measured at the Environment and Climate Change Canada Alsek River above Bates River hydrometric station (navy blue). Dashed line represents the hydrological rerouting (see Shugar and others (2017)) in May of 2016 when runoff from the Kaskawulsh River headwaters was routed to the Alsek River basin. Modelled annual discharge from the Kaskawulsh River headwaters (red) are shown from 2016 onwards only, since contributions to the Alsek Basin were minimal prior to the rerouting event (Shugar and others, 2017). Discharge data from the Alsek River were extracted from the Environment and Climate Change Canada Historical Hydrometric Data web site (https:wateroffice.ec.gc.camainmenuhistorical_data_index_e.html) on 2024-02-16.

4.2 Average monthly discharge on the Alsek River compared to the Kaskawulsh River headwaters

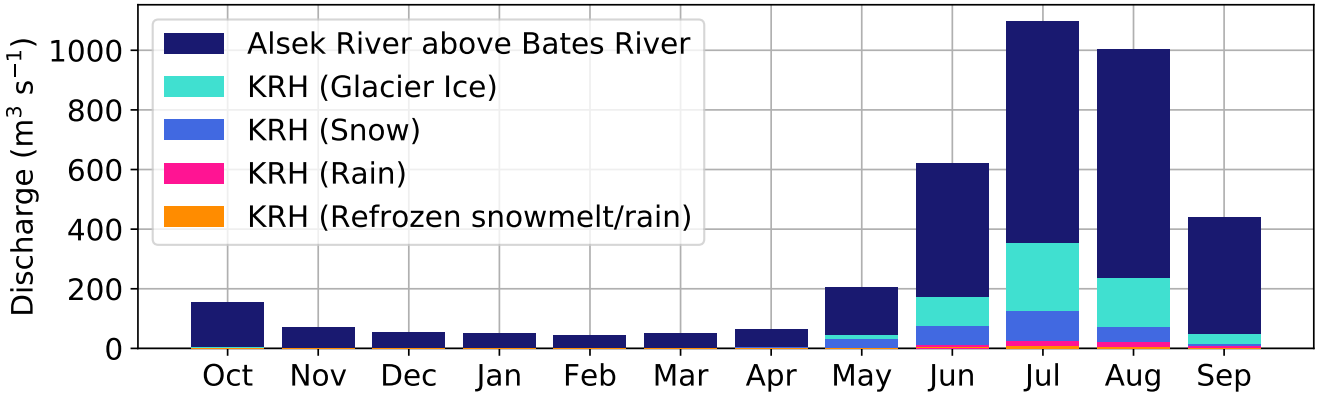

Fig. S4. Mean monthly discharge ($m^3 s^{-1}$) from 2016–2019 at the Alsek River above Bates River hydrometric station (dark blue bars) and mean monthly discharge from the Kaskawulsh River Headwaters (KRH), separated into sources from glacier ice, snow, rain, and refrozen ice. KRH discharge bars are stacked, i.e., total discharge from KRH is the top of the turquoise bars. Monthly discharge data from the Alsek River were extracted from the Environment and Climate Change Canada Historical Hydrometric Data web site (https:wateroffice.ec.gc.camainmenuhistorical_data_index_e.html) on 2024-02-16.

4.3 Decadal-average monthly discharge on the Alsek River

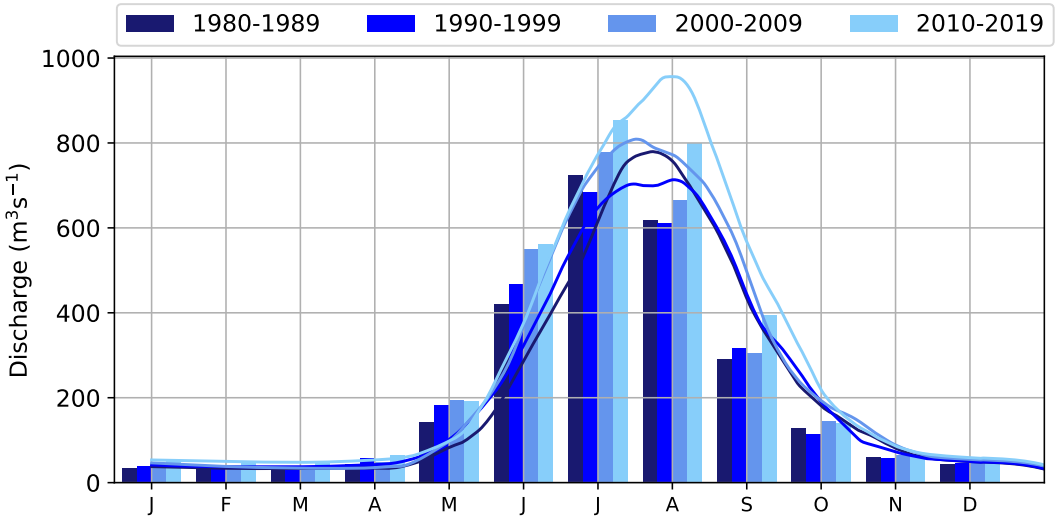

Fig. S5. Mean monthly discharge (bars) measured at the Alsek River above Bates River hydrometric station for each decade in the study period, with decadally averaged daily discharge (lines) smoothed using a zero-phase-shift filter and a window size of 51 days (see Supp. Mat. Section 7). Monthly and daily discharge data from the Alsek River were extracted from the Environment and Climate Change Canada Historical Hydrometric Data web site (https:wateroffice.ec.gc.camainmenuhistorical_data_index_e.html) on 2024-02-16.

5 MANN-KENDALL TEST RESULTS

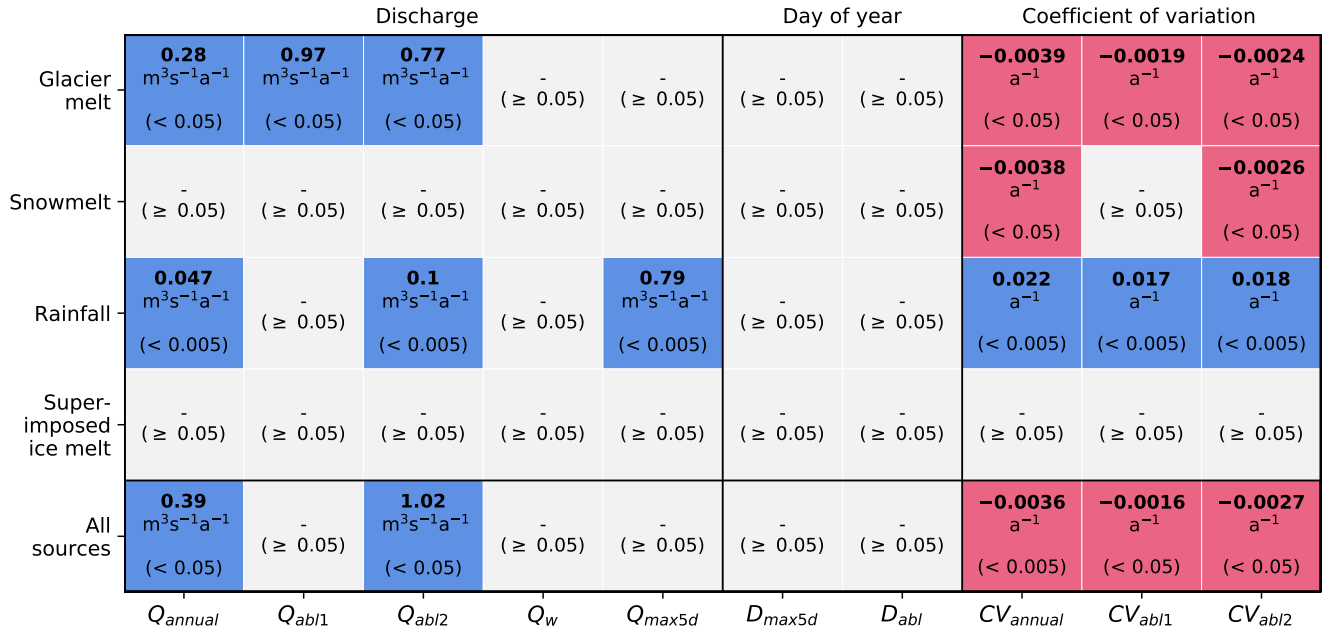

Fig. S6. Results of the original Mann-Kendall test applied to the computed discharge variables (see Table 1 in main text). Blue squares indicate a statistically-significant positive trend over time, while red squares indicate a statistically-significant negative trend over time. Grey squares indicate no statistically-significant trend. Values reported inside each square are the magnitude of the trend (for statistically-significant trends only), while the value in brackets is the p-value.

6 TRENDS IN THE 1980–2022 CLIMATE AND MASS BALANCE

6.1 Seasonal temperature and accumulation

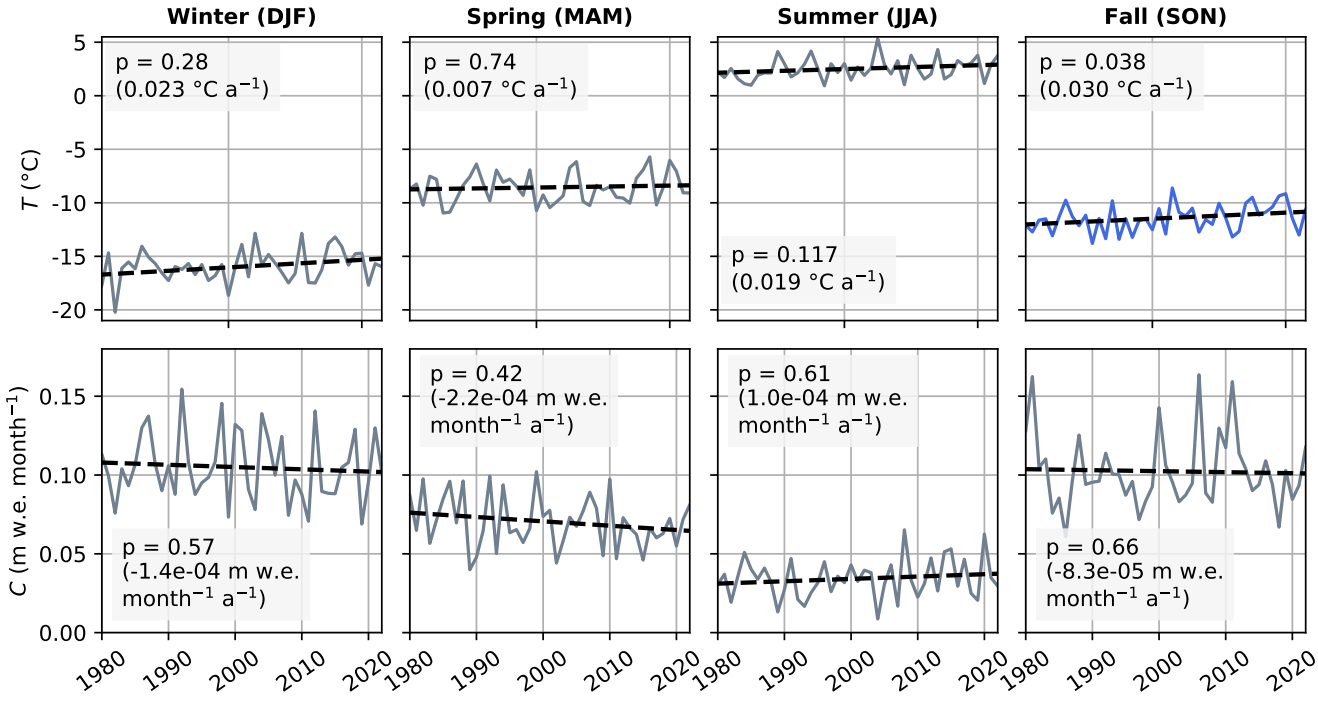

Fig. S7. Mean seasonal air temperature (top row) and seasonal accumulation (bottom row) computed from downscaled and bias-corrected North American Regional Reanalysis (NARR) data. p values represent the statistical significance of the trend determined using the Modified Mann-Kendall test. Statistically significant trends (based on a p value $\leqslant 0.05$) are coloured blue, while non-statistically significant trends are grey. Values in brackets in each panel are the magnitude of the trend, estimated using the Sen's slope. Black dashed lines are a linear regression through the data.

6.2 Annual climate and mass-balance variables

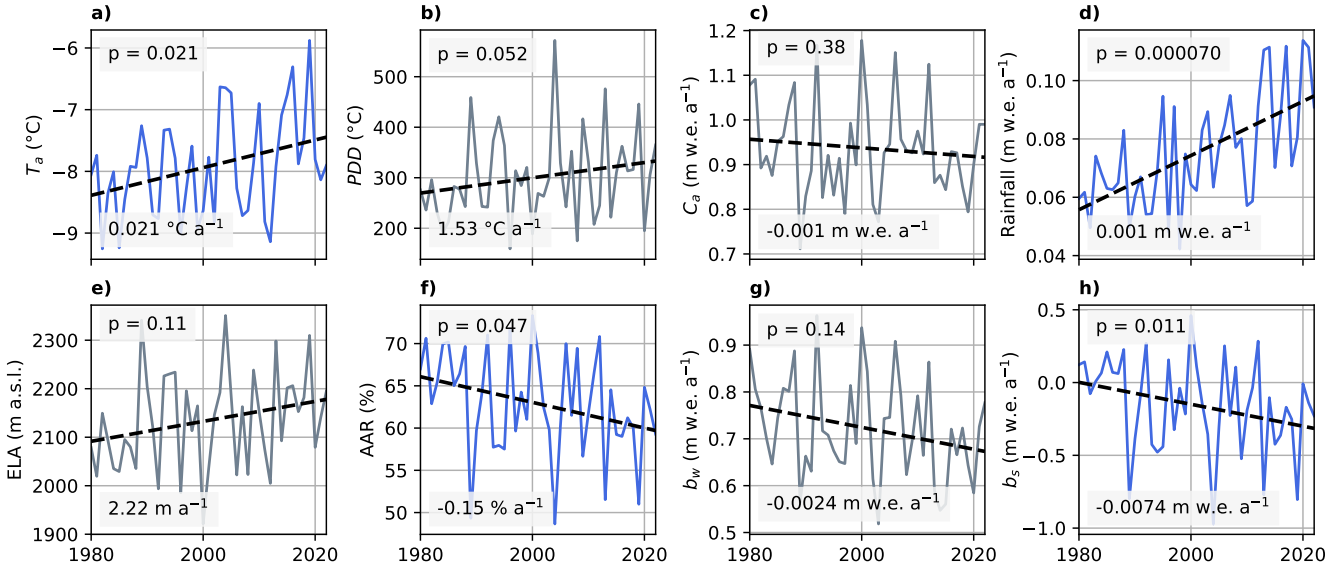

Fig. S8. Annual climate and mass-balance trends. a) Mean annual air temperature, b) positive-degree days, c) mean annual accumulation, d) mean annual rainfall, e) equilibrium line altitude, f) accumulation area ratio, g) winter balance (Cogley and others, 2010), and h) summer balance (Cogley and others, 2010).

6.3 Catchment-wide decadal discharge

	Glacier-ice melt ($km^3\,a^{-1}$)	Snowmelt ($km^3\,a^{-1}$)	Rainfall ($km^3\,a^{-1}$)	Refrozen snowmelt/ rain ($km^3\,a^{-1}$)	Total discharge ($km^3\,a^{-1}$)
1980–1989	1.00 ± 0.32	0.56 ± 0.20	0.09 ± 0.004	0.04 ± 0.11	1.69 ± 0.64
1990–1999	1.09 ± 0.35	0.57 ± 0.21	0.10 ± 0.004	0.04 ± 0.11	1.80 ± 0.68
2000–2009	1.25 ± 0.39	0.61 ± 0.22	0.12 ± 0.004	0.04 ± 0.12	2.01± 0.74
2010–2019	1.27 ± 0.39	0.58 ± 0.21	0.14 ± 0.004	0.04 ± 0.11	2.02 ± 0.72
2020–2022	1.20 ± 0.38	0.64 ± 0.24	0.15 ± 0.006	0.05 ± 0.13	2.04 ± 0.76
1980–2022	**1.15 ± 0.36**	**0.58 ± 0.21**	**0.11 ± 0.004**	**0.04 ± 0.11**	**1.89 ± 0.70**

Table S1. Modelled annual catchment-wide discharge partitioned by source for the Kaskawulsh River headwaters. Uncertainties reported are the standard deviations of the 100 simulations comprising the model.

7 AVERAGE DECADAL DISCHARGE AND SMOOTHING APPROACH

We estimate changes in the magnitude and timing of peak annual discharge by comparing decadally average hydrographs (Figure SS9). Daily discharge is averaged over a 10-year period and smoothed using a zero-phase-shift filter to reduce the noise from interannual variability. We explored a range of window sizes for filter to reduce noise in the data while still preserving the shape of the hydrograph. A window size of 51 days smooths the data while preserving the magnitude and shape of the hydrographs for glacier ice, snow, refrozen ice, and total discharge, as assessed by eye. For rainfall, a window size of 91 days is used to achieve a similar smoothing (Figure SS9). The discharge curves shown in Figure SS9 are the same as those in Figure 6 of the main text.

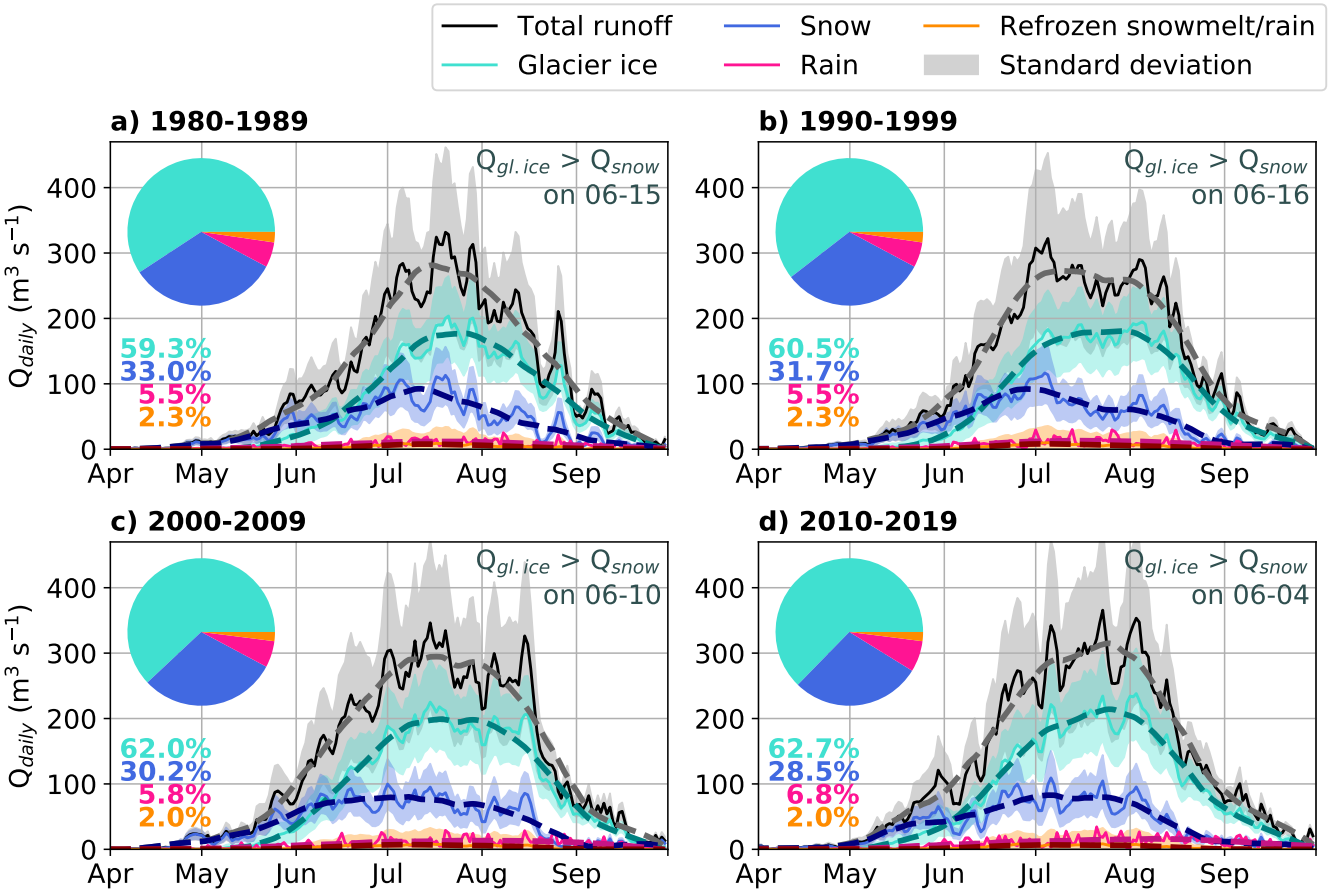

Fig. S9. Catchment-wide daily discharge ($m^3 s^{-1}$) (thin solid lines) averaged over a) 1980–1990, b) 1990–2000, c) 2000–2010, and d) 2010–2020. Thick dashed lines are discharge timeseries smoothed using a zero-phase-shift filter and a window size of 51 (91 for rain). Pie chart and percentages represent fractional contributions from each source to total discharge. Dates printed in top right of each panel are the estimated date when $Q_{gl.ice}$ exceeds Q_{snow} (format MM-DD). The discharge curves shown in here are the same as those in Figure 6 of the main text.

8 EXTREME MASS-BALANCE YEARS AND THE SUBSEQUENT WATER BUDGETS

8.1 Negative mass-balance years

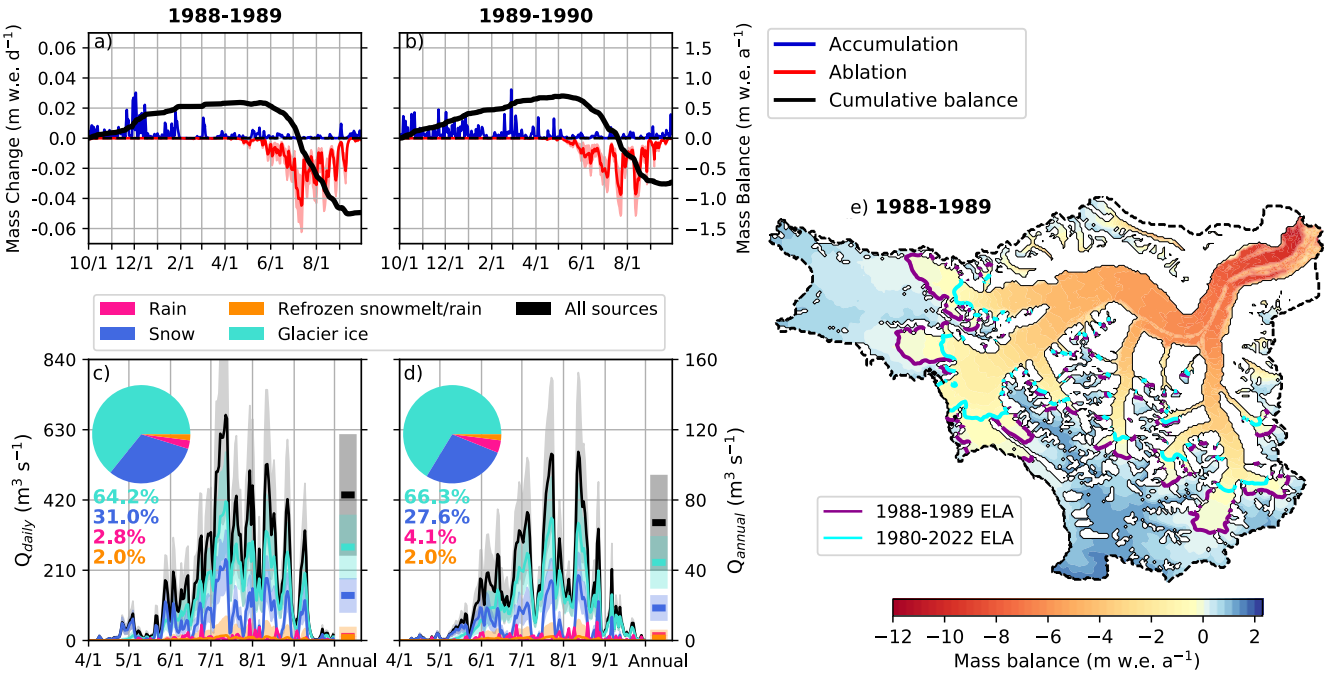

Fig. S10. Mass balance and water budgets corresponding to (a,c) 1988-1989 (one the most negative mass-balance year between 1980–2022), and (b,d) the following year. (e) The distributed mass balance for the 1988-1989 hydrological year (1 Oct–30 Sept), with the 1988-1989 modelled ELA (purple line) compared to the long-term modelled ELA (cyan line).

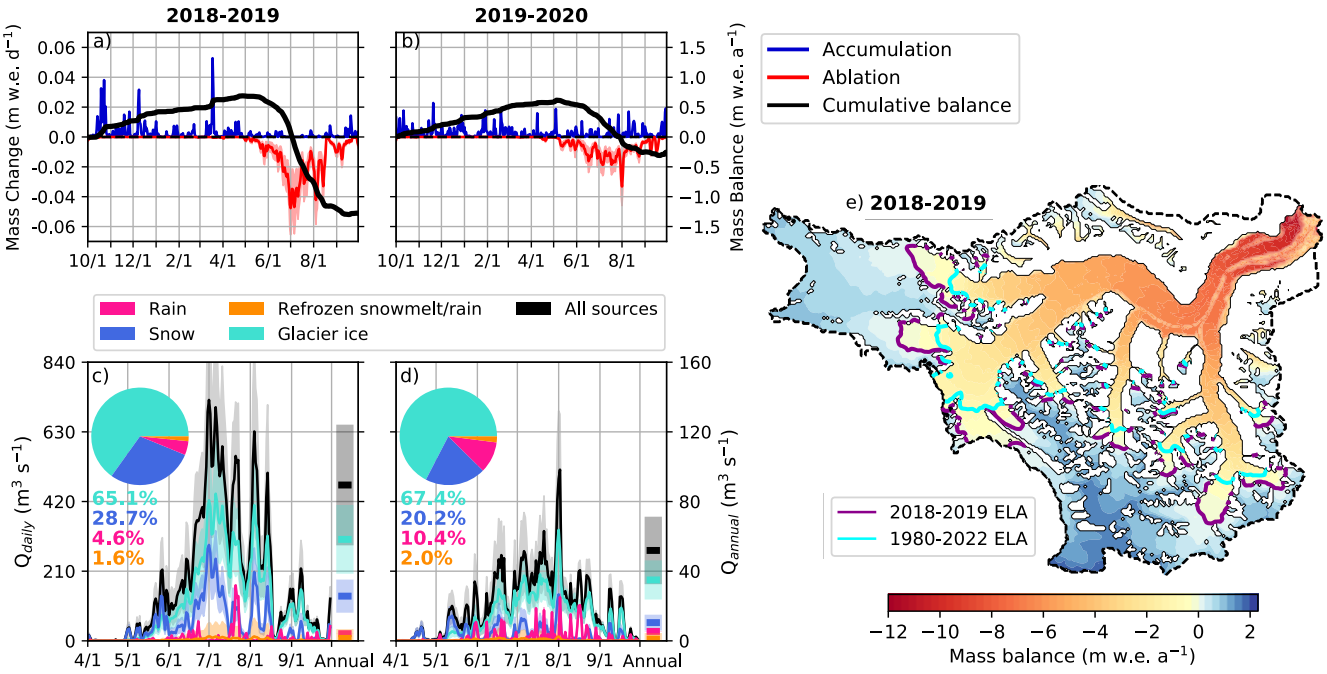

Fig. S11. Mass balance and water budgets corresponding to (a,c) 2018-2019 (one the most negative mass-balance year between 1980–2022), and (b,d) the following year. (e) The distributed mass balance for the 2018-2019 hydrological year (1 Oct–30 Sept), with the 2018-2019 modelled ELA (purple line) compared to the long-term modelled ELA (cyan line).

8.2 Positive mass-balance years

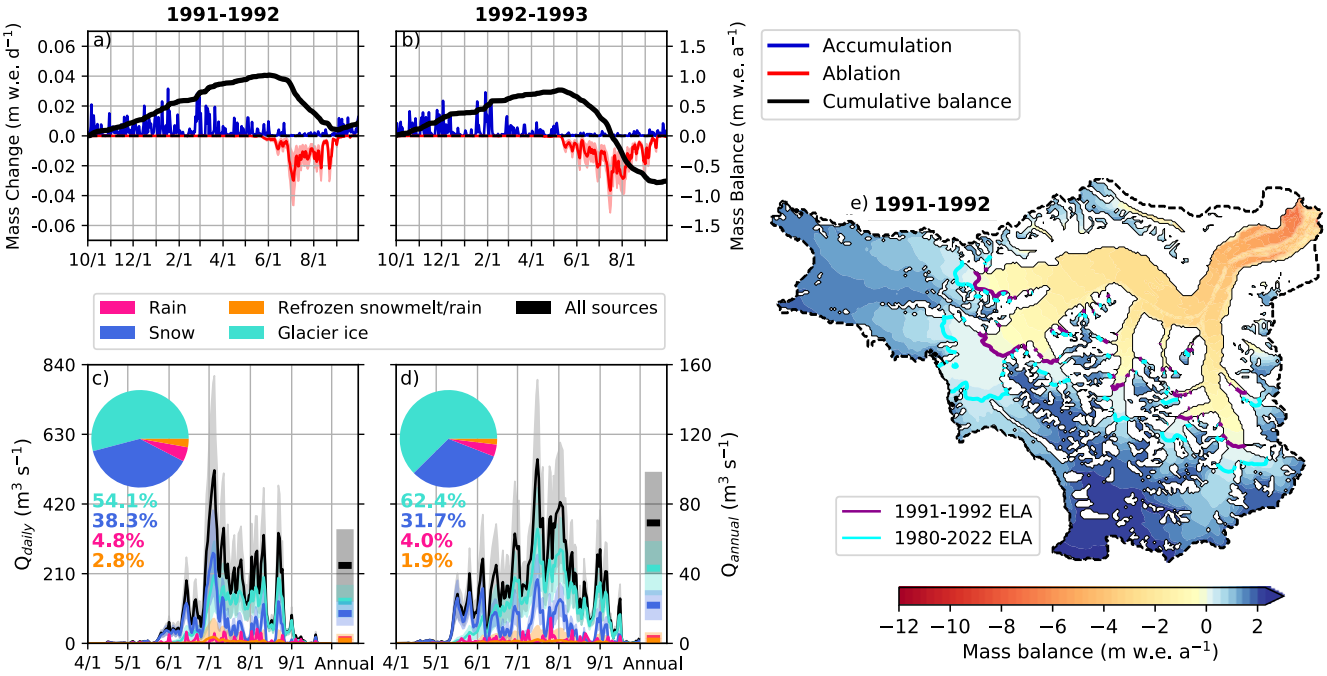

Fig. S12. Mass balance and water budgets corresponding to (a,c) 1991-1992 (one the most positive mass-balance year between 1980–2022), and (b,d) the following year. (e) The distributed mass balance for the 1991-1992 hydrological year (1 Oct–30 Sept), with the 1991-1992 modelled ELA (purple line) compared to the long-term modelled ELA (cyan line).

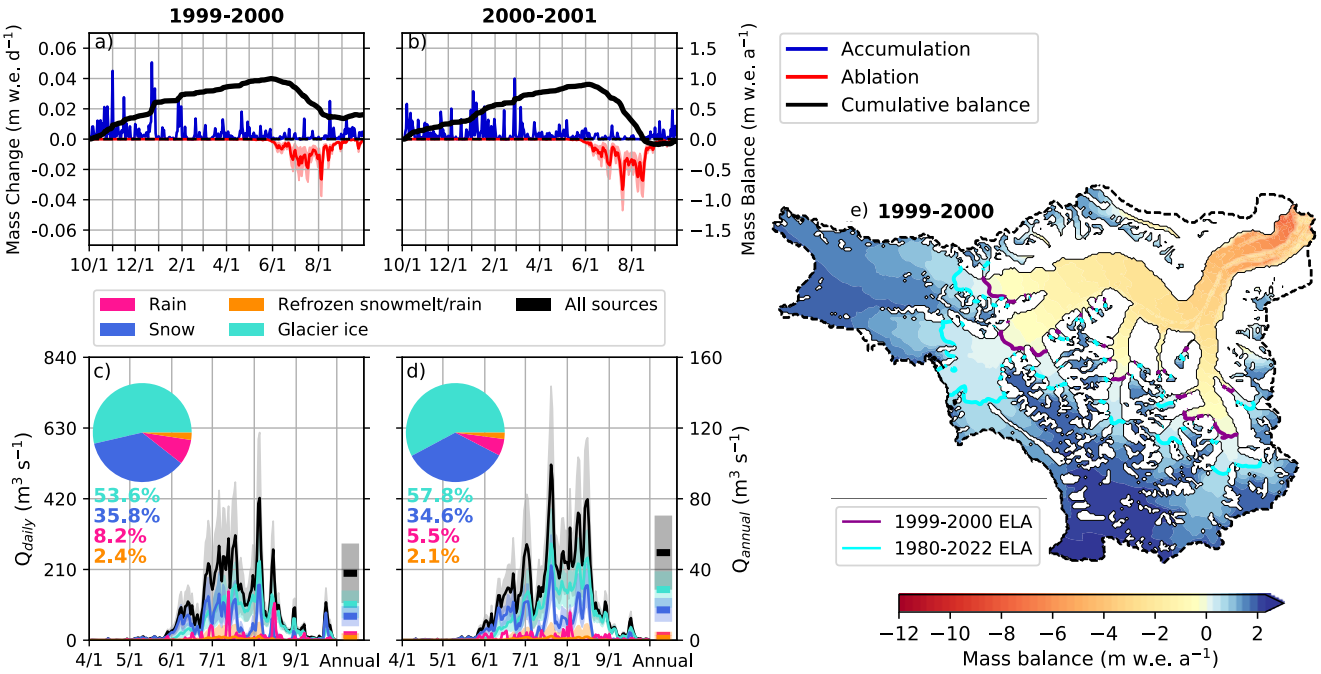

Fig. S13. Mass balance and water budgets corresponding to (a,c) 1999-2000 (one the most positive mass-balance year between 1980–2022), and (b,d) the following year. (e) The distributed mass balance for the 1999-2000 hydrological year (1 Oct–30 Sept), with the 1999-2000 modelled ELA (purple line) compared to the long-term modelled ELA (cyan line).

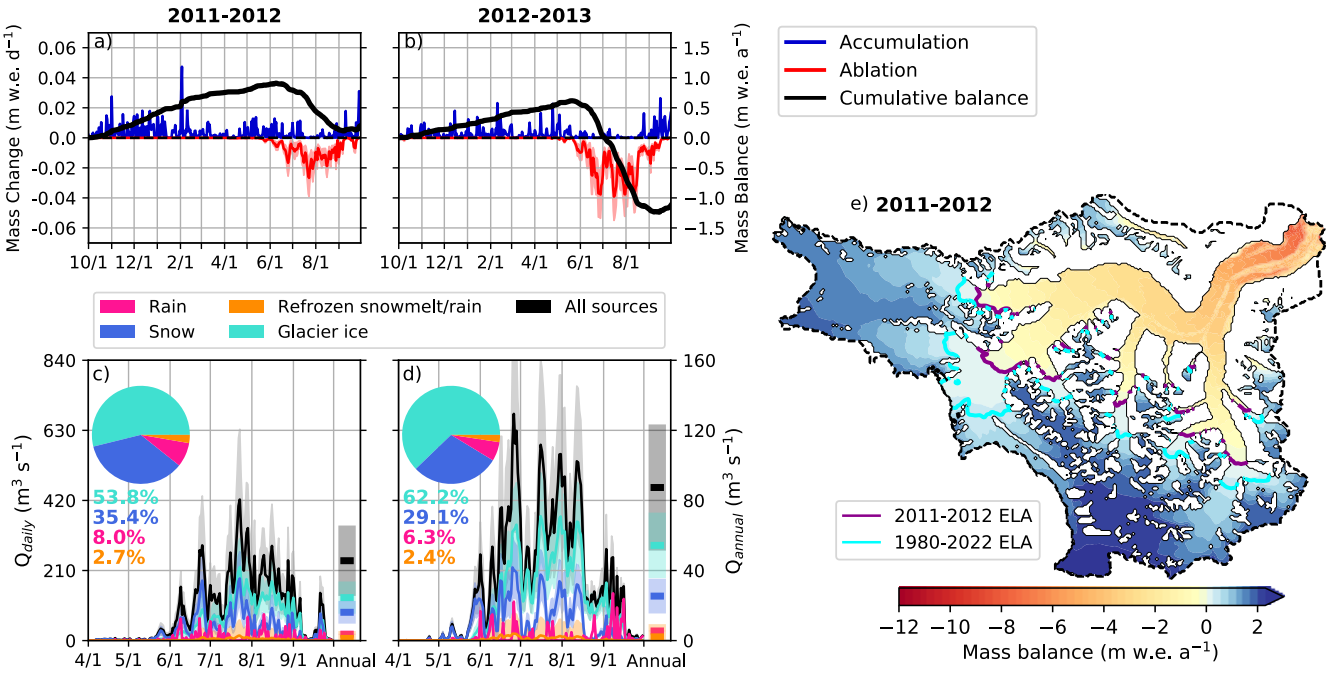

Fig. S14. Mass balance and water budgets corresponding to (a,c) 2011-2012 (one the most positive mass-balance year between 1980–2022), and (b,d) the following year. (e) The distributed mass balance for the 2011-2012 hydrological year (1 Oct–30 Sept), with the 2011-2012 modelled ELA (purple line) compared to the long-term modelled ELA (cyan line).

9 MODEL SENSITIVITY TO CLIMATE

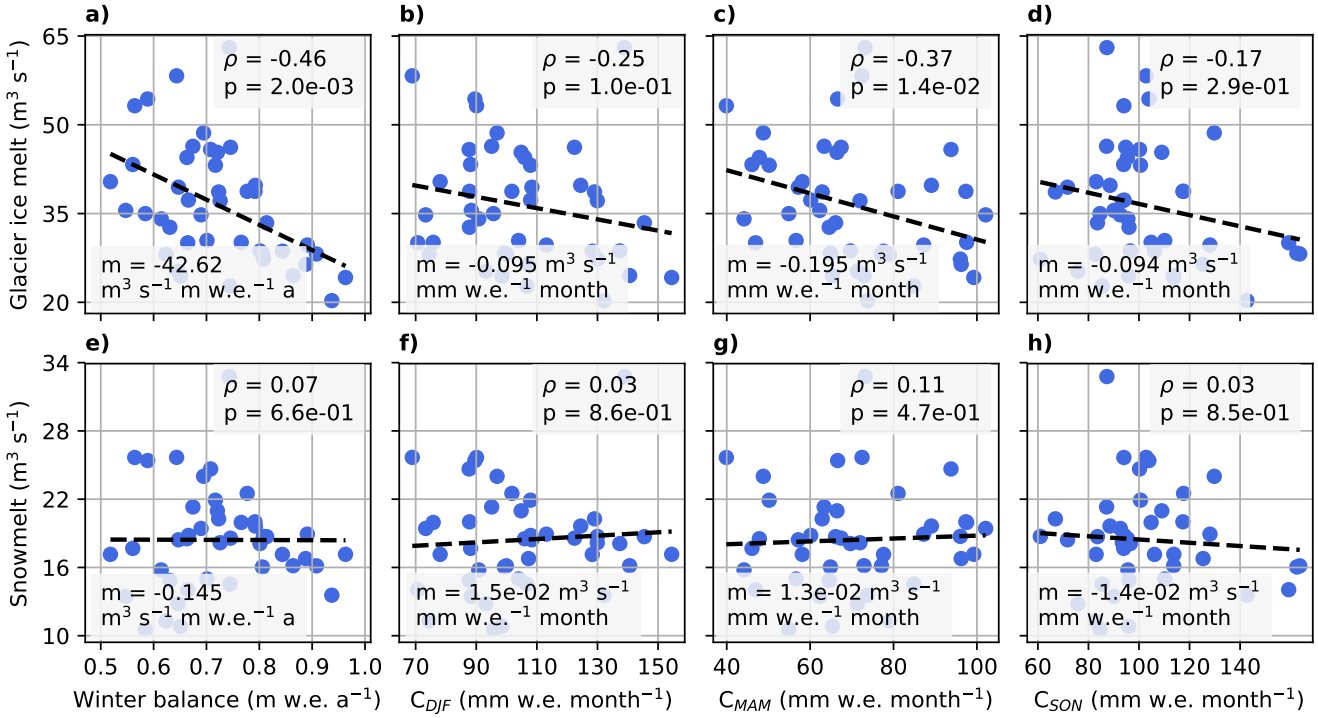

Fig. S15. Relationships between modelled discharge from glacier ice melt (a–d) or snowmelt (e–h) and: (a,e) winter balance, (b,f) winter accumulation (C_{DJF}), (c,g) spring accumulation (C_{DJF}), and (d,h) fall accumulation (C_{DJF}), fitted with a linear regression. ρ is the Spearman's correlation coefficient, p is the p-value from Spearman's correlation test, and m is the slope of the linear regression (dashed line).

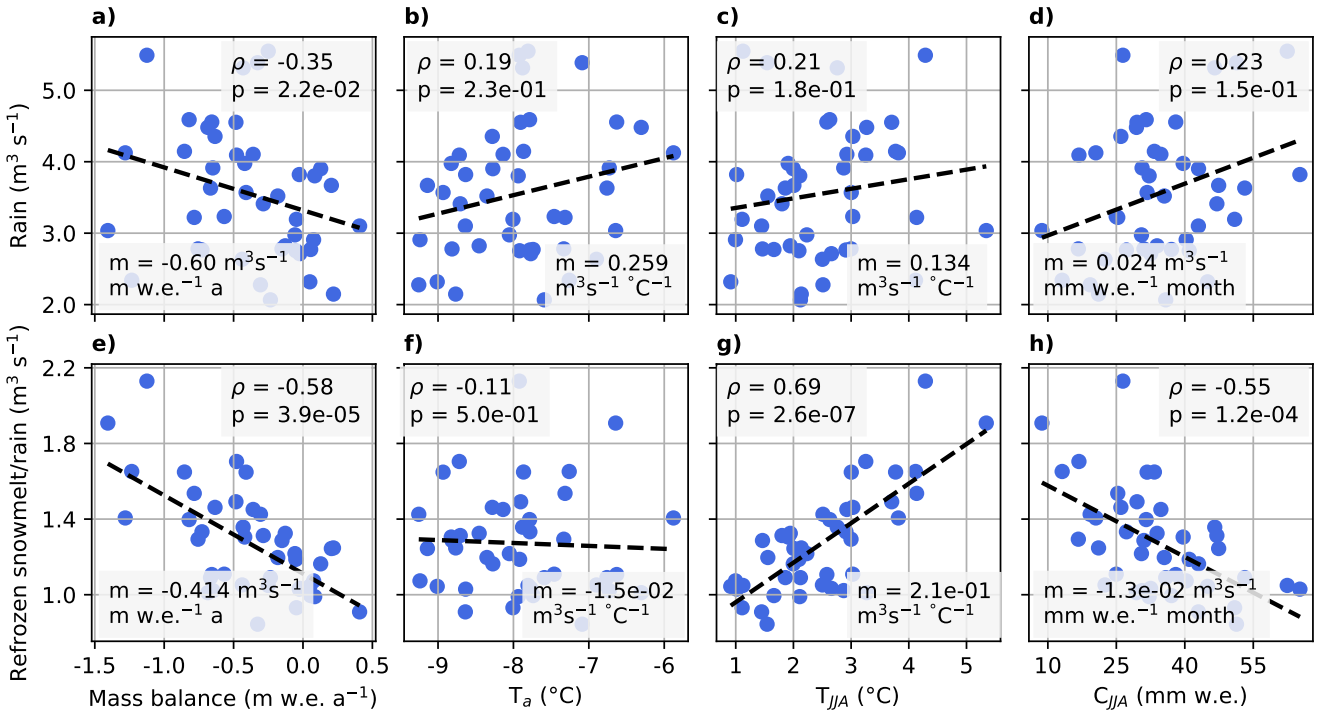

Fig. S16. Relationships between modelled discharge from rainfall (a–d) or melt from refrozen snowmelt/rain (e–h) and: (a,e) mass balance, (b,f) mean annual air temperature (T_a), (c,g) mean summer air temperature (T_{JJA}), and (d,h) total summer accumulation (C_{JJA}), fitted with a linear regression. ρ is the Spearman's correlation coefficient, p is the p-value from Spearman's correlation test, and m is the slope of the linear regression (dashed line).

REFERENCES

Cogley JG, Arendt A, Bauder A, Braithwaite R, Hock R, Jansson P, Kaser G, Moller M, Nicholson L, Rasmussen L and others (2010) Glossary of glacier mass balance and related terms. *IHP-VII Technical Documents in Hydrology No. 86, IACS Contribution No. 2, UNESCO-IHP, Paris.*

Cuffey KM and Paterson WSB (2010) *The physics of glaciers*. Academic Press

Hock R (1999) A distributed temperature-index ice-and snowmelt model including potential direct solar radiation. *Journal of Glaciology*, **45**(149), 101–111 (doi: 10.3189/S0022143000003087)

Huybrechts P and De Wolde J (1999) The dynamic response of the Greenland and Antarctic ice sheets to multiple-century climatic warming. *Journal of Climate*, **12**(8), 2169–2188

Janssens I and Huybrechts P (2000) The treatment of meltwater retention in mass-balance parameterizations of the Greenland ice sheet. *Annals of Glaciology*, **31**, 133–140 (doi: 10.3189/172756400781819941)

Shugar DH, Clague JJ, Best JL, Schoof C, Willis MJ, Copland L and Roe GH (2017) River piracy and drainage basin reorganization led by climate-driven glacier retreat. *Nature Geoscience*, **10**(5), 370–375 (doi: 10.1038/ngeo2932)

Young EM, Flowers GE, Berthier E and Latto R (2021) An imbalancing act: the delayed dynamic response of the Kaskawulsh Glacier to sustained mass loss. *Journal of Glaciology*, **67**(262), 313–330 (doi: 10.1017/jog.2020.107)